Spin-orbit coupling induced anisotropy effects in bimetallic antiferromagnets: A route towards antiferromagnetic spintronics

A. B. Shick,[1] S. Khmelevskyi,[2] O. N. Mryasov,[3] J. Wunderlich,[4] and T. Jungwirth[5,6]
[1]*Institute of Physics, ASCR, v.v.i., Na Slovance 2, 182 21 Praha 8, Czech Republic*
[2]*CMS, Vienna University of Technology, Makartvilla, Gusshausstr. 25, 1040 Vienna, Austria*
[3]*MINT, University of Alabama, Tuscaloosa, Alabama 35487, USA*
[4]*Hitachi Cambridge Laboratory, Cambridge CB3 0HE, United Kingdom*
[5]*Institute of Physics, ASCR, v.v.i., Cukrovarnická 10, 162 53 Praha 6, Czech Republic*
[6]*School of Physics and Astronomy, University of Nottingham, Nottingham NG7 2RD, United Kingdom*
(Received 17 May 2010; published 24 June 2010)

Magnetic anisotropy phenomena in bimetallic antiferromagnets Mn_2Au and MnIr are studied by first-principles density-functional theory calculations. We find strong and lattice-parameter-dependent magnetic anisotropies of the ground-state energy, chemical potential, and density of states, and attribute these anisotropies to combined effects of large moment on the Mn 3*d* shell and large spin-orbit coupling on the 5*d* shell of the noble metal. Large magnitudes of the proposed effects can open a route towards spintronics in compensated antiferromagnets without involving ferromagnetic elements.

DOI: 10.1103/PhysRevB.81.212409 PACS number(s): 75.45.+j, 75.50.Cc, 85.75.Mm

The introduction in 1991 of a hard-drive read-head based on the ferromagnetic anisotropic magnetoresistance (AMR) effect represented a major step in the field which later on became known as spintronics.[1–3] The basic physics of the AMR, namely, the bulk nature of this magnetotransport effect and its subtle spin-orbit coupling (SOC) origin, have limited the magnitude of the effect and the potential of scaling the AMR devices into small dimensions required for current high-density magnetic storage applications. These limitations were partly overcome by the discovery of the giant magnetoresistance (GMR) and tunneling magnetoresistance (TMR) effects which are interface transport phenomena and which rely primarily on mutual orientation of two magnetic electrodes. One of the scenarios that may lead to next breakthroughs in the field of spintronics foresees a replacement of ferromagnetic electrodes by antiferromagnets (AFMs). The rigidity to external magnetic fields and the absence of stray fields make AFMs particularly favorable materials for ultrafast and ultrahigh-density spintronics. To date, studies of magnetoresistive effects potentially suitable for AFM spintronics have focused on AFM counterparts to the GMR.[4–6] While the viability of this approach is yet to be discerned it has been acknowledged that the requirements on the structural quality and the coherence of transport through interfaces in the GMR devices are significantly more stringent in the case of AFMs.

This Brief Report aims to open an alternative route towards AFM spintronics which reintroduces the leading role of SOC. In this approach, the stringent requirements on the GMR/TMR are circumvented by considering instead the tunneling AMR (TAMR) and the Coulomb-blockade AMR (CBAMR) effects. We also demonstrate that SOC can be employed to control magnetic anisotropies in the AFM in a way that leads to reorientation of the staggered moments required for observing the above anisotropic transport effects.

Previous studies of the TAMR (Refs. 7–11) and CBAMR (Refs. 12 and 13) in ferromagnets have shown that anisotropic magnetoresistance phenomena can be extended from bulk to nanoscale devices, can have large magnitudes and do not require spin-coherent transport throughout the structure. In transition-metal ferromagnets a generic principle has been outlined, based on studies of magnetocrystalline anisotropies and of the TAMR and CBAMR,[11,12,14] that the magnetic anisotropy phenomena are maximized in bimetallic systems combining large spontaneous moments on the 3*d* shell of a transition metal and large magnetic susceptibility and SOC on the 5*d* shell of a noble metal. Since Mn carries the largest moment among transition metals and most of the bimetallic alloys containing Mn order antiferromagnetically, the goals of strong magnetic anisotropy phenomena and of AFM spintronics appear to merge naturally together. In our relativistic *ab initio* study we consider the Mn_2Au AFM for which recent theoretical calculations predicted[15] record Néel temperature (>1500 K) among Mn-based AFM alloys. The generic nature of the proposed anisotropy phenomena is confirmed by calculations in the conventional bimetallic AFM MnIr.

We begin with a detail analysis of magnetocrystalline anisotropies in Mn_2Au. It has been reported to be paramagnetic,[16] and at the threshold of itinerant electron magnetism. Later it was shown[15] that this material is AFM with well-localized moments on the Mn atoms. This AFM transition was not observed in experiment[16] since its Néel temperature is higher than peritectoid temperature, and low-temperature metamagnetic behavior can be related to small number of anticite Mn atoms on Au-atoms positions.

The calculations are performed considering the $MoSi_2$-type body-centered-tetragonal structure with experimental lattice parameters, $a=6.291$ a.u. and $c=16.142$ a.u. The tetragonal unit cell with two formula units (f.u.) and an AFM arrangement of magnetic moments are shown in Fig. 1. This staggered magnetic structure was obtained from the theoretical study[15] of the magnetic interactions, and leads to the AFM stacking of the Mn layers with no frustration.

We employ the relativistic version of the full-potential linearized augmented-plane wave (FP-LAPW) method in the

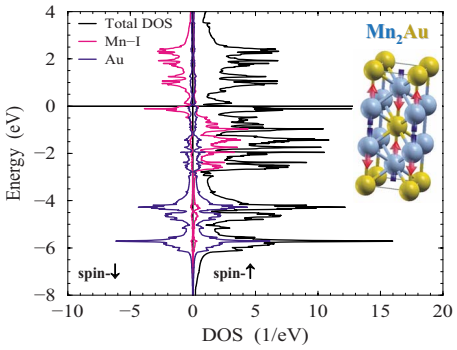

FIG. 1. (Color online) Total DOS (per f.u.), spin-resolved Au-atom and Mn-atom projected DOSs, and a schematic view of the crystal and AFM structure of Mn_2Au. (Mn-I denotes one of two Mn sublattices with opposite spin polarizations.)

local spin-density (von Barth-Hedin) approximation. The SOC is included in a self-consistent second-variational procedure.[17] This approach is typically very accurate for itinerant metallic systems. The calculated total and atom resolved density of states (DOS) for moments aligned with the [001] axis are shown in Fig. 1. We find that Mn atoms carry spin $M_S = \pm 3.2\mu_B$ and orbital $M_L = \mp 0.013\mu_B$ magnetic moments and there are no magnetic moments on the Au atoms. When staggered magnetization is aligned along the [100]/[010] axis there is no change in M_S of Mn and the magnitude of $|M_L| = 0.007\mu_B$ is reduced.

The magnetocrystalline anisotropy energy (MAE) is evaluated using the torque method which is implemented in the FP-LAPW basis.[14] For the tetragonal symmetry case, the phenomenological total energy dependence on the spin-quantization direction reads,

$$E(\theta,\phi) = K_{2\perp}\sin^2\theta + K_{4\perp}\sin^4\theta + K_{4\parallel}\sin^4\theta\cos 4\phi \tag{1}$$

and the corresponding torque is given by $T(\theta,\phi) = dE(\theta,\phi)/d\theta = \sin 2\theta[K_{2\perp} + 2(K_{4\perp} + K_{4\parallel}\cos 4\phi)\sin^2\theta]$. Here $K_{2\perp}$ is the uniaxial MAE constant, and $K_{4\perp}$ and $K_{4\parallel}$ are the fourth-order out-of-plane MAE constants and in-plane MAE constants, respectively. The advantage of this approach is that it allows us to split the total MAE into the element-specific contributions from different atoms in the unit cell. The total and element-specific anisotropy constants are shown in Table I. The convergence better than 0.01 meV/f.u. with respect to the number of k points in the Brillouin zone was achieved for a set of 6875 k points.

The largest uniaxial anisotropy constant, $K_{2\perp}$, is strong and clearly dominated by contributions from the Au sublattice. The leading role in the MAE of Au atoms which carry zero net moment may appear counterintuitive and requires more detail inspection. In the AFM state the Au orbitals point towards the neighboring Mn moments with opposite orientations and strong hybridization between Mn and Au creates oppositely polarized parts of the Au orbitals. Considering separately exchange fields produced by the two Mn sublattices, $\alpha = \uparrow, \downarrow$, with opposite strongly localized moments

TABLE I. Relativistic full-potential density-functional theory calculations of the uniaxial K_2, and fourth-order out-of-plane, and in-plane $K_{4\perp}$, $K_{4\parallel}$ MAE constants (total and element specific in meV per f.u.) of Mn_2Au. Additional uniaxial MAE $K^*_{2\parallel}$ (in meV per f.u. per 1% strain) is induced by in-plane strain along the [100] crystal direction (see text).

	$K_{2\perp}$	$K_{4\perp}$	$K_{4\parallel}$	$K^*_{2\parallel}$
Mn_2Au	−2.44	0.02	0.01	0.07
Au	−2.72	0.01	0.01	0.08
Mn_2	0.28	0.01	0.00	−0.01

$(\pm\mathbf{M}^{3d})$, each of the sublattices induces magnetic moment $\mathbf{M}^{5d}_{\alpha}$ on the itinerant $5d$ electrons of Au atoms. We can write[14,18]

$$\mathbf{M}^{5d}_{\alpha} = \chi\sum_i J^{i,\alpha}_{3d\text{-}5d}\mathbf{M}^{3d}_{\alpha,i}, \tag{2}$$

where we sum over the Mn atoms in the sublattice α, $J^{i,\alpha}_{3d\text{-}5d}$ is the exchange interaction between the ith Mn atom from the sublattice α and the Au atom, and χ is the local spin susceptibility of the Au atom. Strong SOC on Au yields the MAE contributions due to $\mathbf{M}^{5d}_{\uparrow,\downarrow}$. For the uniaxial term it can be written as $E^{5d}_{A,\alpha} = -k^{5d}_{2\perp}(M^{5d,z}_{\alpha})^2$, where the renormalized anisotropy constant $k^{5d}_{2\perp}$ is proportional to the square of the SOC parameter ξ^2_{5d}. Using Eq. (2) we can write,

$$E^{5d}_{A,\alpha} = -k^{5d}_2\chi^2\sum_{ij} J^{i,\alpha}_{3d\text{-}5d}J^{j,\alpha}_{3d\text{-}5d}M^{3d,z}_{\alpha,i}M^{3d,z}_{\alpha,j}. \tag{3}$$

Summing Eq. (2) over the Mn sublattices α, we get zero magnetic moment which complies with the overall time-reversal symmetry of the AFM band structure. The total MAE due to Au, $\Sigma_{\alpha=\uparrow,\downarrow}E^{5d}_{A,\alpha}$, is nonzero, however, as seen from Eq. (3). It originates from a combination of strong $5d$ SOC $(k^{5d}_{2\perp})$, strong exchange splitting induced by the $3d$ magnetic element $(J_{3d\text{-}5d}\mathbf{M}^{3d})$, and the enhancement of the local spin susceptibility χ. Equation (3) implies that MAE is predominantly governed by two-site anisotropy and is proportional to the number of bonds between the Au and Mn atoms.

Large magnetocrystalline anisotropies in bimetallic AFMs have already been reported in *ab initio* studies of the common AFM MnIr. The key role of polarized orbitals of the noble metal has not, however, been identified in these works. To test that the physics described in the previous paragraph is generic, we have examined the element-specific MAE of MnIr. In the calculations we considered the experimental lattice constants of the $L1_0$ MnIr and the unit cell with 2 f.u. in a checkerboard collinear AFM structure.[19,20] For the total MAE $(K_{2\perp} + K_{4\perp} + K_{4\parallel})$ we obtained −3.365 meV/f.u. (−6.73 meV per unit cell). This number is in good agreement with previous results (−7.05 meV per unit cell in Ref. 19 and −6.81 meV per unit cell in Ref. 20). Our element-specific decomposition of the MAE shows that, similarly to the case of Mn_2Au, the MAE is dominated by the contribution from the noble metal which again carries zero net moment in MnIr. For the leading uniaxial MAE term $K_{2\perp}$ we

obtained a contribution of −3.38 meV/f.u. from Ir and a much weaker contribution of 0.024 meV/f.u. from Mn.

We now turn to the discussion of the magnetotransport effects in AFMs. The AMR effects are even in magnetic moment and, similar to the MAE, can be finite in the compensated AFM. In what follows we provide estimates of the AMR in the Coulomb blockade and tunneling regimes. To date TAMR and CBAMR have been observed only in ferromagnets. We argue that both these effects are present and can be large in compensated AFMs.

The CBAMR builds on a general principle that transport through an electronic device depends on positions of electrochemical potentials in the relevant electrodes. Transport and band structure with SOC are in this case directly linked via the anisotropy of the chemical potential with respect to the orientation of magnetic moments.[12,21] Single-electron transistors (SETs) are arguably the most sensitive devices to detect this effect. Large magneto-Coulomb oscillations of the conductance are induced by rotating magnetic moments, whenever the changes in the chemical potential become comparable to the single-electron charging energy of the central island in the SET.[12] Our calculated difference between chemical potentials for the staggered magnetization aligned along the [110] axis and the [001] axis is −2.5 meV for Mn_2Au and 3.2 meV for MnIr. This is comparable to chemical-potential anisotropies in ferromagnetic semiconductor (Ga,Mn)As and in bimetallic ferromagnets.[12] The AFM CBAMR or a magnetoresistance of other AFM devices which are sensitive to changes in electrochemical potentials on the order of a few millivolts should therefore be readily detectable.

For FM tunneling devices it has been demonstrated that a useful qualitative analysis of the differential TAMR can be obtained by considering its proportionality to the energy-dependent anisotropy in the density of states (ADOS) in the magnetic electrode with respect to the crystallographic orientation of magnetic moments.[7,9] Recent model studies of the TAMR for ferromagnets[22] provide further proof for the validity of the DOS anisotropy approximation for the TAMR ratio. We assume that it is equally valid for AFMs. Anisotropy in the group-velocity weighted tunneling density of states (ATDOS) is considered instead of the ADOS when referring to tunnel junctions with high-quality interfaces, i.e., high degree of in-plane momentum conservation during tunneling.[7,9] We emphasize that in either case these calculations are only approximate as they neglect the anisotropy of tunneling matrix elements between wave functions in the magnetic and nonmagnetic electrodes of the TAMR structure.[23]

Calculated energy-dependent ADOS and ATDOS for Mn_2Au and staggered moments aligned with the easy [110] and hard [001] staggered magnetization axes are plotted in Fig. 2(a). The ADOS can be as high as 50% in the vicinity of the Fermi level and oscillates strongly with energy. This implies a sizable TAMR whose magnitude and sign are bias dependent, similar to the experimentally observed TAMR characteristics in bimetallic ferromagnets.[10,11] The calculated ATDOS is also large and shows weaker dependence on energy around the Fermi level. In MnIr the ADOS between the easy [100] and hard [001] staggered magnetization axes is

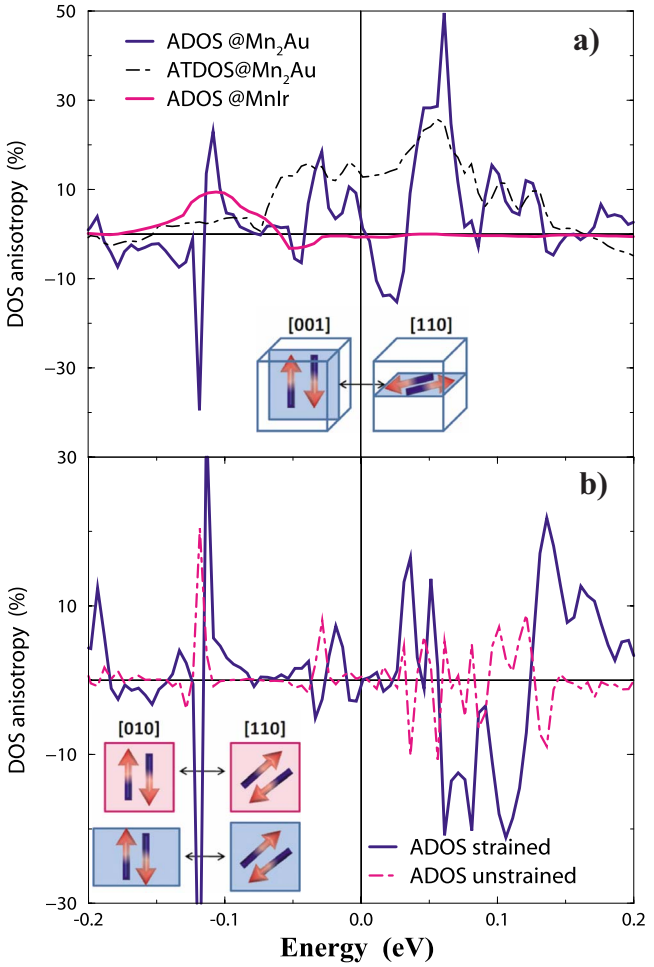

FIG. 2. (Color online) (a) DOS anisotropies for the hard ([001]) and easy ([110]) axes of Mn_2Au, and the hard ([001]) and easy ([100]) axes of MnIr. (b) In-plane DOS anisotropies for staggered moment aligned along the easy axis ([010]) of the strained Mn_2Au crystal and along the easy axis ([110]) of the unstrained Mn_2Au. The energy is measured from the Fermi level.

weaker but still reaching 10%, as shown in Fig. 2(a). Note that for staggered moment reorientations between the easy and hard axes, MnIr is expected to display weaker TAMR of the two considered AFMs while the corresponding magnetic anisotropy constant $K_{2\perp}$ and the anisotropy in the chemical potential are stronger in MnIr. This illustrates that despite their common SOC origin the different magnetic anisotropy phenomena can behave to some extent independently.

The absence of a net magnetization makes AFMs rigid to magnetic fields and therefore one needs to resort to manipulation of the staggered moments via internal fields. One approach, previously reported in the literature, is based on exchange-spring effects[24] occurring when the AFM is interfaced with a ferromagnet. This technique can be used to trigger the reorientation between the easy [110] axis and hard [001] axes which produces the TAMR effects predicted in Fig. 2(a). Instead of this exchange field method we now return to the magnetocrystalline anisotropy and demonstrate that the staggered moments can be controlled via this internal field without involving ferromagnets. Specifically we consider the dependence of the MAE and of the corresponding

in-plane easy-axis orientation in the AFM on the lattice strain. (This can be controlled externally by, e.g., a piezoelectric stressor.[25])

As shown in Table I, the in-plane easy axis of unstrained Mn_2Au lies along the [110] (or $[1\bar{1}0]$) crystal direction. By applying a sufficiently strong strain along one of the cube edges, the easy axis, and therefore also the staggered moments, will rotate towards the [100] or [010] direction, depending on the sign of the strain. To model this effect we elongated/contracted the unit cell along the [100]/[010] axis, keeping the unit-cell volume fixed. The corresponding crystal structure becomes orthorhombic and the second-order uniaxial anisotropy terms are given by $\sin^2\theta[K_{2\perp}+K^*_{2\parallel}\cos 2\phi]$.

Assuming strains up to 1% we found negligible changes in the out-of-plane uniaxial constant $K_{2\perp}$ and in the fourth-order constants $K_{4\perp}$ and $K_{4\parallel}$. For the strain-induced in-plane uniaxial MAE we obtained $K^*_{2\parallel}=0.07$ meV/f.u. per 1% strain and again the dominant contribution comes from the Au atom (0.08 meV/f.u. per 1%). The easy-axis shifts from the in-plane diagonal to the [010] direction when $K_{2\parallel}>2K_{4\parallel}$. It means that only a fraction of a percent strain is required to rotate the staggered moments between the [110] and [010] axes. These crystallographic directions are nonequivalent in the tetragonal Mn_2Au and can yield a sizable TAMR, as shown by the corresponding in-plane ADOS in Fig. 2(b). Note that the detailed TAMR characteristics can be modified by the strain as illustrated by the other ADOS curve in Fig. 2(b) which corresponds to the relative difference between the DOS in the unstrained case and moments along the [110] axis, and the DOS in 1% strained case and moments along the [010] axis. Nevertheless, the primary role of the strain is in the MAE where it triggers the reorientation of the magnetic easy axis.

In conclusion, we have proposed a set of relativistic magnetoresistance effects which can open a route towards AFM spintronics and which can be realized in AFMs alone without involving ferromagnetic elements. Our previous works in which TAMR and CBAMR were predicted for transition-metal ferromagnets[9,12] using similar relativistic *ab initio* techniques have been subsequently confirmed by experiments.[10,11,13] This together with the identified microscopic physics behind the magnetic anisotropy effects in compensated AFMs gives us confidence that predictions presented in this Brief Report are realistic.

We acknowledge stimulating discussions with Bryan Gallagher, Allan MacDonald, and Jan Mašek, and financial support from EU under Grants No. FP7-215368 SemiSpinNet, No. FP7-214499 NAMASTE, Austrian Grant MOEL OEFG, Czech Republic under Grants No. GACR ON/06/E001, No. FON/06/E002, No. GACR P204/10/0330, No. GAAV IAA100100912, No. AV0Z10100520, No. AV0Z10100521, No. KAN400100652, and No. LC510, and Premium Academiae.

[1] M. N. Baibich, J. M. Broto, A. Fert, F. Nguyen Van Dau, F. Petroff, P. Etienne, G. Creuzet, A. Friederich, and J. Chazelas, Phys. Rev. Lett. **61**, 2472 (1988).
[2] G. Binasch, P. Grunberg, F. Saurenbach, and W. Zinn, Phys. Rev. B **39**, 4828 (1989).
[3] C. Chappert, A. Fert, and F. Nguyen Van Dau, Nature Mater. **6**, 813 (2007).
[4] A. S. Núñez, R. A. Duine, P. Haney, and A. H. MacDonald, Phys. Rev. B **73**, 214426 (2006).
[5] P. M. Haney, D. Waldron, R. A. Duine, A. S. Núñez, H. Guo, and A. H. MacDonald, Phys. Rev. B **75**, 174428 (2007).
[6] R. A. Duine, P. M. Haney, A. S. Núñez, and A. H. MacDonald, Phys. Rev. B **75**, 014433 (2007).
[7] C. Gould, C. Rüster, T. Jungwirth, E. Girgis, G. M. Schott, R. Giraud, K. Brunner, G. Schmidt, and L. W. Molenkamp, Phys. Rev. Lett. **93**, 117203 (2004).
[8] L. Brey, C. Tejedor, and J. Fernández-Rossier, Appl. Phys. Lett. **85**, 1996 (2004).
[9] A. B. Shick, F. Máca, J. Mašek, and T. Jungwirth, Phys. Rev. B **73**, 024418 (2006).
[10] L. Gao, X. Jiang, S.-H. Yang, J. D. Burton, E. Y. Tsymbal, and S. S. P. Parkin, Phys. Rev. Lett. **99**, 226602 (2007).
[11] B. G. Park, J. Wunderlich, D. A. Williams, S. J. Joo, K. Y. Jung, K. H. Shin, K. Olejník, A. B. Shick, and T. Jungwirth, Phys. Rev. Lett. **100**, 087204 (2008).
[12] J. Wunderlich, T. Jungwirth, B. Kaestner, A. C. Irvine, A. B. Shick, N. Stone, K. Y. Wang, U. Rana, A. D. Giddings, C. T. Foxon, R. P. Campion, D. A. Williams, and B. L. Gallagher, Phys. Rev. Lett. **97**, 077201 (2006).
[13] A. Bernand-Mantel, P. Seneor, K. Bouzehouane, S. Fusil, C. Deranlot, F. Petroff, and A. Fert, Nat. Phys. **5**, 920 (2009).
[14] A. B. Shick, F. Máca, M. Ondráček, O. N. Mryasov, and T. Jungwirth, Phys. Rev. B **78**, 054413 (2008).
[15] S. Khmelevskyi and P. Mohn, Appl. Phys. Lett. **93**, 162503 (2008).
[16] S. Abe, M. Matsumoto, T. Kaneko, H. Yoshida, H. Morita, and T. Kanomata, J. Magn. Magn. Mater. **140-144**, 103 (1995).
[17] A. B. Shick, D. L. Novikov, and A. J. Freeman, Phys. Rev. B **56**, R14259 (1997).
[18] O. N. Mryasov, U. Nowak, K. Y. Guslienko, and R. W. Chantrell, Europhys. Lett. **69**, 805 (2005).
[19] R. Y. Umetsu, A. Sakuma, and K. Fukamichi, Appl. Phys. Lett. **89**, 052504 (2006).
[20] L. Szunyogh, B. Lazarovits, L. Udvardi, J. Jackson, and U. Nowak, Phys. Rev. B **79**, 020403 (2009).
[21] M. Tran, J. Peiro, H. Jaffres, J. M. George, O. Mauguin, L. Largeau, and A. Lemaître, Appl. Phys. Lett. **95**, 172101 (2009).
[22] A. Matos-Abiague and J. Fabian, Phys. Rev. B **79**, 155303 (2009).
[23] J. Moser, A. Matos-Abiague, D. Schuh, W. Wegscheider, J. Fabian, and D. Weiss, Phys. Rev. Lett. **99**, 056601 (2007).
[24] A. Scholl, M. Liberati, E. Arenholz, H. Ohldag, and J. Stöhr, Phys. Rev. Lett. **92**, 247201 (2004).
[25] A. W. Rushforth *et al.* Phys. Rev. B **78**, 085314 (2008).